UCLA
UCLA Previously Published Works

Title

Experimental determination of CePO4 and YPO4 solubilities in H2O–NaF at 800°C and 1 GPa: implications for rare earth element transport in high-grade metamorphic fluids

Permalink

https://escholarship.org/uc/item/67g6d485

Journal

Geofluids, 13(3)

ISSN

1468-8115

Authors

Tropper, P
Manning, CE
Harlov, DE

Publication Date

2013-08-01

DOI

10.1111/gfl.12031

Peer reviewed

eScholarship.org Powered by the California Digital Library
University of California

GEOFLUIDS

Geofluids (2013) **13**, 372–380 doi: 10.1111/gfl.12031

Experimental determination of $CePO_4$ and YPO_4 solubilities in H_2O–NaF at 800°C and 1 GPa: implications for rare earth element transport in high-grade metamorphic fluids

P. TROPPER[1,2], C. E. MANNING[2] AND D. E. HARLOV[3]

[1]*Institute of Mineralogy and Petrography, Faculty of Geo- and Atmospheric Sciences, University of Innsbruck, Innsbruck, Austria;* [2]*Department of Earth and Space Sciences, University of California, Los Angeles, CA, USA;* [3]*Helmholtz Zentrum Potsdam, Deutsches GeoForschungsZentrum, Potsdam, Germany*

ABSTRACT

Monazite ($CePO_4$) and xenotime (YPO_4) are important accessory minerals in metasediments. They host significant rare earth elements (REE) and are useful for geochronology and geothermometry, so it is essential to understand their behavior during the metasomatic processes that attend high-grade metamorphism. It has been proposed that F-bearing fluids enhance solubility and mobility of REE and Y during high-grade metamorphism. We assessed this possibility by determining the solubility of synthetic $CePO_4$ and YPO_4 crystals in H_2O–NaF fluids at 800°C and 1 GPa. Experiments used hydrothermal piston-cylinder and weight-loss methods. Compared to the low solubilities of $CePO_4$ and YPO_4 in pure H_2O (0.04 ± 0.04 and 0.25 ± 0.04 millimolal, respectively), our results indicate an enormous increase in the solubility of both phosphates with increasing NaF concentration in H_2O: $CePO_4$ solubility reaches 0.97 molal in 20 mol.% NaF, and YPO_4 shows an even stronger solubility enhancement to 0.45 molal in only 10 mol.% NaF. The greatest relative solubility increases occur at the lowest NaF concentration. The solubilities of $CePO_4$ and YPO_4 show similar quadratic dependence on NaF, consistent with possible dissolution reactions of: $CePO_4 + 2NaF = CeF_2^+ + Na_2PO_4^-$ and $YPO_4 + 2NaF = YF_2^+ + Na_2PO_4^-$. Solubilities of both REE phosphates are significantly greater in NaF than in NaCl at equivalent salt concentration. A fluid with 10 mol.% NaCl and multiply saturated with fluorite, $CePO_4$, and YPO_4 would contain 1.7 millimolal Ce and 3.3 millimolal Y, values that are respectively 2.1–2.4 times greater than in NaCl-H_2O alone. The results indicate that Y, and by extension heavy rare earth elements (HREE), can be fractionated from LREE in fluorine-bearing saline brines which may accompany granulite-facies metamorphism. The new data support previous indications that REE/Y mobility at these conditions is enhanced by complexing with F in the aqueous phase.

Key words: brines, monazite, piston-cylinder experiments, rare earth elements mobility, solubility, xenotime

Received 13 August 2012; accepted 8 March 2013

Corresponding author: Peter Tropper, Institute of Mineralogy and Petrography, Faculty of Geo- and Atmospheric Sciences, University of Innsbruck, Innrain 52, A-6020 Innsbruck, Austria.
Email: peter.tropper@uibk.ac.at. Tel: 0043-(0)512-507-5513.

Geofluids (2013) **13**, 372–380

INTRODUCTION

Fluorine plays an important role in metal complexing during fluid–rock interaction at high pressure (*P*) and temperature (*T*). Increased fluorine concentrations are indicated by F-bearing minerals in a wide variety of deep metamorphic settings (Bohlen & Essene 1978; Zhu & Sverjensky 1992; Pradeepkumar & Krishnanath 1996; Markl & Piazzolo 1998; Tsunogae *et al.* 2003; Sengupta *et al.* 2004). Fluorine-rich fluids can strongly influence the distribution of Ti and other high field-strength elements (HFSE), rare earth elements (REE; light rare earth elements, LREE; heavy rare earth elements, HREE), and U and Th during metamorphism and partial melting (Oreskes & Einaudi 1990; Peterson *et al.* 1991; Pan & Fleet 1996; Rudnick *et al.* 2000; Klemme 2004; Jiang *et al.* 2005; Rapp *et al.* 2010). The mobilities of REE in crustal and mantle fluids are especially important because of their role in REE ore-deposit formation (Andreoli *et al.* 1994; Fayek & Kyser 1997; Salvi *et al.* 2000; Chakhmouradian & Wall 2012; Williams-Jones *et al.* 2012) as well as their contribution in tracing magmatic (Pollard *et al.* 1987; Webster *et al.*

© 2013 John Wiley & Sons Ltd

1997; Markl & Piazolo 1998; Agangi *et al.* 2010) and metamorphic (Yardley 1985; Brennan 1993) petrogenetic processes. The same holds for Y because of its geochemical similarity to Ho. Unfortunately, little is known about the actual F content of high-grade metamorphic fluids. Most studies inferred relative fHF/fH_2O ratios based on halogen partitioning between minerals and fluids to make inferences about the fluid compositions (Yardley 1985; Zhu & Sverjensky 1992; Markl & Piazolo 1998; Sallet 2000). Direct measurements of F contents are mostly available from geothermal fluids (Lewis *et al.* 1997) and not from high-grade metamorphic fluids. Banks *et al.* (1994) analyzed a magmatic fluid with high total REE concentrations of 200–1300 ppm and found a strong correlation with increasing F contents (360–5250 ppm), which suggests the transport of REE as F-bearing complexes.

Important reservoirs for REE and Y in crustal rocks are the phosphates apatite, monazite, and xenotime, as well as the epidote-group minerals. Most previous work on REE/Y solubility in geofluids has focused on monazite and/or xenotime because of their stoichiometric simplicity, their importance as low- to medium-grade metamorphic index minerals, and their utility as geochronological tools (Harrison *et al.* 2002; Ayers *et al.* 2004; Hansen & Harlov 2007; Williams *et al.* 2007; Janots *et al.* 2008). Most experimental investigations of their solubilities in aqueous fluids have been conducted at low to moderate *P* and *T* (Wood *et al.* 1990a,b; Haas *et al.* 1995; Devidal *et al.* 1998; Poitrasson *et al.* 2004; Cetiner *et al.* 2005; Migdisov & Williams-Jones 2007; Migdisov *et al.* 2009; Pourtier *et al.* 2010). However, the links between REE mobility and F may be especially important in high-*P* environments (Pan & Fleet 1996; Cooper *et al.* 2012). Experimental studies of monazite and xenotime solubility at these conditions confirm that they are sparingly soluble in pure H_2O (Ayers & Watson 1991; Schmidt *et al.* 2007; Tropper *et al.* 2011). Although solubilities rise with increasing X_{NaCl} (Tropper *et al.* 2011), the role of the potentially more important halide, F, has not yet been investigated. The need for such an investigation is highlighted by the compositions of metamorphic fluorites, which display different REE/Y fractionation behavior as a function of fluid composition (Constantopoulos 1988; Bau & Dulski 1995; Schwinn & Markl 2005).

Here, we report measurements of $CePO_4$ and YPO_4 solubility in H_2O–NaF at 800°C and 1.0 GPa, which yields insights into F-related REE mobility that is commonly observed to be associated with granulite-facies metamorphism (Pan & Fleet 1996; Harlov *et al.* 2006). The new data indicate that $CePO_4$ and YPO_4 solubilities are extremely high in NaF-bearing fluids. We used NaF solutions rather than HF solutions to avoid the consequences of imposing acidic pH at the studied P and T. These results indicate that in the presence of even small concentrations of dissolved alkali fluoride, geologic fluids will have a high capacity to dissolve and transport REE at high *P* and *T*.

METHODS

We used a double-capsule method and the synthetically grown, chemically pure $CePO_4$ and YPO_4 crystals whose synthesis is described in the study by Tropper *et al.* (2011). One to 15 small crystals free of flux-melt inclusions were placed in an inner 1.6-mm outer diameter (OD) Pt capsule. To facilitate H_2O penetration during experiments, the capsule was pierced two to four times with a needle and then lightly crimped on both ends to contain the crystal. The inner capsule, appropriate amounts of dried NaF, and 25–42 ml H_2O were then sealed by arc welding in an outer 3.5-mm OD Pt capsule with 0.18 mm wall thickness. The double-capsule assembly was held at 115°C for $\geq$3 h to check for leakage.

All experiments were conducted in an end-loaded, piston-cylinder apparatus using 25.4-mm-diameter graphite–NaCl furnace assemblies (Bohlen 1984; Manning & Boettcher 1994). Each capsule, packed in NaCl, was placed horizontally in the inner part of the assembly in contact with the thermocouple tip through a Pt shield in order to prevent puncture by the thermocouple. Temperature was controlled with $Pt/Pt_{90}Rh_{10}$ thermocouples ($\pm$3°C estimated precision), and pressure was monitored using a Heise gauge ($\pm$0.01 GPa estimated precision). The run time was 12 h, which has been shown by Tropper *et al.* (2011) to be sufficient for equilibration.

Power to the apparatus was cut at the end of each experiment, causing quench to temperatures <100°C in $\leq$30 sec. After quenching, the outer capsule was pierced with a needle, dried for 15 min at 115°C, and then for 15 min at 400°C. The capsule assembly was then opened and inspected. The crystals were extracted and weighed. Comparison of the total capsule weight before and after the experiments showed that H_2O loss during runs was always within 1% of starting H_2O. All run products were examined optically with a binocular microscope; selected run products were examined with a scanning electron microscope. The extracted crystals were carefully dried and cleaned prior to weighing.

Crystal weights were determined using a Mettler UMX2 ultra-microbalance (1σ = 0.2 μg). Weights of NaF and H_2O were determined using a Mettler M4 microbalance (1σ = 2 μg). Uncertainties in $CePO_4$ and YPO_4 solubilities reflect propagated weighing errors (Table 1).

RESULTS

Results are given in Table 1. Run products included partly dissolved starting crystals and fine-grained white or

Table 1 Experimental results at 800°C, 1 GPa.

Run	Time (h)	H_2O in (mg)	NaF in (mg)	X_{NaF}	Crystals in (mg)	Crystals out (mg)	Molality	Notes
$CePO_4 + H_2O + NaF$								
Mnz-18	90	35.893	0	0	1.1635	1.1632	0.00004 (3)	T11
Mnz-9	12	40.956	0.976	0.010	1.2751	1.2683	0.0007 (1)	
Mnz-8	12	34.304	4.451	0.053	1.0927	0.7147	0.0469 (1)	
Mnz-10	12	34.856	8.798	0.098	4.9013	3.4928	0.1719 (1)	VT?
Mnz-14	12	36.302	20.814	0.197	10.3721	2.1349	0.9652 (1)	
Mnz-4	12	25.590	21.427	0.264	3.2851	–	>0.5461 (1)	
$YPO_4 + H_2O + NaF$								
Xnt-4	12	41.618	0	0	2.3541	2.3522	0.00025 (4)	T11
Xnt-11	12	41.492	1.004	0.010	1.7494	1.7110	0.0050 (1)	
Xnt-10	12	35.206	4.867	0.056	1.2402	0.2842	0.1477 (1)	
Xnt-12	12	34.622	9.086	0.101	6.8693	3.7319	0.4928 (1)	M + V?
Xnt-15	12	34.464	8.927	0.100	5.4425	2.5930	0.4497 (1)	M + V?
Xnt-14	12	36.465	20.837	0.197	10.6652	–	>1.5906 (1)	
Xnt-6	12	25.522	21.509	0.266	3.5388	–	>0.7541 (1)	

Parenthetical entries reflect propagated weighing errors (1σ) in final digit. The 1σ error in X_{NaF} is 1.8×10^{-5}. Notes: T11, data from Tropper *et al.* (2011); VT?, possible vapor-transport crystals; M + V?, possible coexistence of melt + vapor, as indicated by the presence of up to 100-μm-diameter glass spheres in run products (see text).

colorless quench solids, which occur in the inner as well as the outer capsules. The original grains displayed rounded edges and, in some cases, significant new subhedral octahedral overgrowths (Figs 1A,B and 2A,B). The absence of any other crystalline products of dissolution indicates that monazite and xenotime dissolved congruently in all solutions.

As noted in previous studies (Tropper & Manning 2005; Antignano & Manning 2008), it is important to identify any phosphate crystals that might have nucleated and grown during an experiment. Termed 'vapor-transport crystals', these newly formed grains have habits consistent with growth at high *P* and *T* rather than during quenching. Their presence results in erroneously high solubilities if they are unrecognized. In one experiment, Mnz-10, several small clusters of equant, subhedral monazite grains (Fig. 1C) were assumed to be vapor-transport crystals; however, the dependence of monazite solubility on NaF concentration does not change significantly when this experiment is omitted from fitting (see below). Accordingly, we conclude that the mass of these possible vapor-transport crystals was negligible.

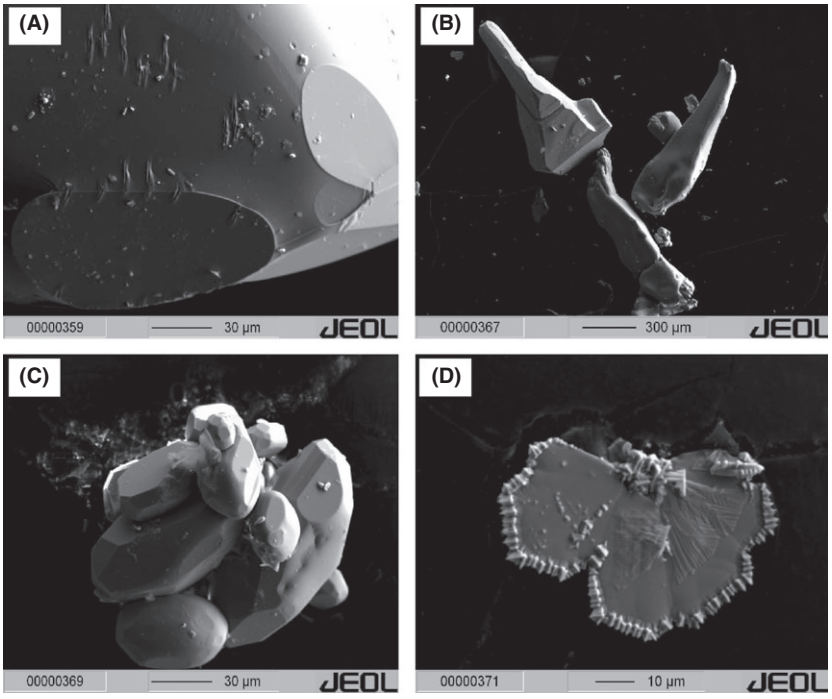

Fig. 1. Backscatter electron (BSE) images of reaction products from the $CePO_4$–H_2O–NaF solubility experiments. (A) Image of a $CePO_4$ starting crystal after the experiment showing dissolution grooves and recrystallization faces of $CePO_4$ starting crystals at $X_{NaF} = 0.05$ (Mnz-8). (B) Recrystallized remnants of $CePO_4$ crystals at $X_{NaF} = 0.1$ (Mnz-10). (C) Small aggregate of possible $CePO_4$ vapor-transport crystals in the $X_{NaF} = 0.1$ experiment (Mnz-10). (D) Quench crystal in the $X_{NaF} = 0.1$ experiment (Mnz-10).

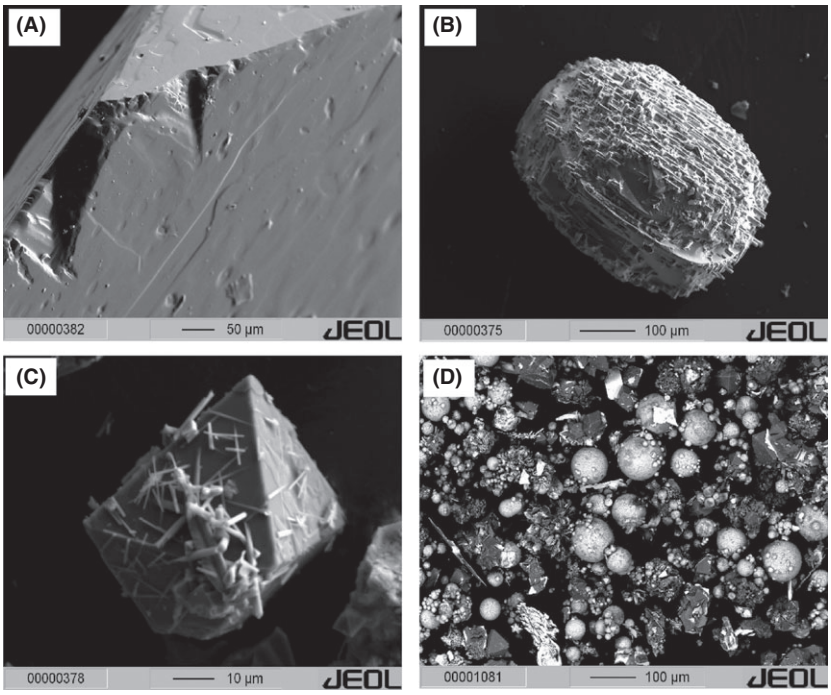

Fig. 2. Backscatter electron (BSE) images of the reaction products of the YPO_4–H_2O–NaF solubility experiments. (A): Image of a YPO_4 starting crystal after the experiment showing dissolution grooves at X_{NaF} = 0.01 (Xnt-11). (B): Recrystallized YPO_4 crystal at X_{NaF} = 0.05 (Xnt-10). (C): Small aggregate of quench crystals on a NaF octahedron in the X_{NaF} = 0.05 experiment (Xnt-10). (D): Large spherules in an X_{NaF} = 0.1 experiment (Xnt-12) indicating possible coexistence of melt + vapor.

Quench phosphate and fluoride crystals were observed in all experiments. They form sheet- to needle-shaped crystals (Figs 1D and 2C). Semiquantitative EDS analysis of a sheet-like quench crystal in experiment Mnz-10 yielded a Ce/F ratio of 1:2. In the outer capsule, NaF crystallizes as cubes as well as octahedrons.

The quenching and drying procedure leads to preservation of quench solutes as minute spheres <10 µm in diameter. However, two experiments (Xnt-12 and Xnt-15) at X_{NaF} = 0.1 yielded larger spheres that were up to approximately 100 µm in diameter and typically coated by smaller spheres (Fig. 2D). These may indicate coexistence of melt + vapor at experimental conditions; however, similar textures were not observed at higher dissolved NaF and YPO_4 concentrations (Table 1).

Quench pH was determined to be 12 in one experiment (Xnt-15; X_{NaF} = 0.1). This strongly alkaline quench pH implies that Na ≫ F in the quench solution. This implies that quench precipitates are richer in fluoride than in Na, yielding excess NaOH in the residual solution.

The solubilities of $CePO_4$ and YPO_4 in pure H_2O are below 1 millimolal at 800°C and 1 GPa (Tropper *et al.* 2011; Table 1). The solubility of both phosphates rises strongly with added NaF (Fig. 3). In the case of $CePO_4$, solubility increases to 0.965 mol kg^{-1} H_2O at X_{NaF} = 0.2 (Fig. 3). In experiment Mnz-4 at X_{NaF} = 0.264, the starting crystal completely dissolved, yielding a minimum solubility of 0.55 molal. Thus, monazite solubility increases by more than approximately 25 000 times over the investigated range. The data were fit to an equation of the form $mi = m_i^\circ + AX_{NaF}^2$, where m_i° is the measured solubility in pure H_2O and A = 24.34 (R^2 = 0.993). The increase in the solubility of YPO_4 with increasing NaF concentration is even stronger, rising to 0.449 mol kg^{-1} H_2O at X_{NaF} = 0.1 (Fig. 3). Complete dissolution of the crystals was again observed at $X_{NaF} \geq 0.2$. Least-squares regression

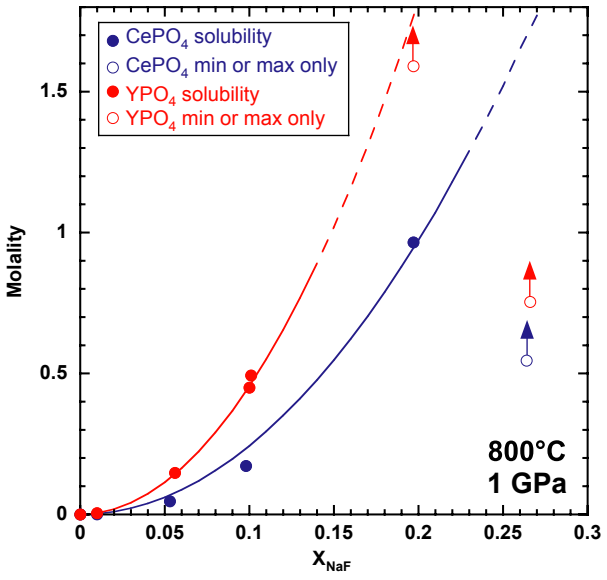

Fig. 3. Measured molalities of $CePO_4$ (blue circles) and YPO_4 (red circles) versus X_{NaF} at 800°C and 1 GPa. Open circles with arrows represent minimum or maximum values only. Error bars (2σ) are smaller than the symbol size. The lines represent the calculated molality based on fit parameters (see text) and are dashed where extrapolated significantly beyond constraints from the experimental data.

of the data to the function above yielded $A = 45.43$ ($R^2 = 0.999$).

DISCUSSION

Solubility trends

Both $CePO_4$ and YPO_4 exhibit a strong solubility increase with a rising NaF concentration (Fig. 3). This behavior mirrors that seen when NaCl solutions are used (Tropper *et al.* 2011); however, the relative increases are substantially greater in NaF compared to NaCl. At a given salt concentration, both $CePO_4$ and YPO_4 are at least 10 times greater in NaF relative to NaCl, even for X_{salt} as low as approximately 0.02 (Fig. 4A,B). Relative solubility enhancements are compared on a mole-fraction basis in Fig. 4C, which shows that even though the YPO_4 solubility is greater than that of $CePO_4$ at a given X_{NaF} (Fig. 3), the increase in the solubility of YPO_4 in NaF solutions relative to that in pure H_2O is not as strong as that for $CePO_4$ (Fig. 4C). This is due to the greater solubility of YPO_4 than that of $CePO_4$ in pure H_2O.

The relative effects of NaF versus NaCl solutions can be compared by ratioing the concentration of dissolved REE phosphate at the same salt mole fraction (Fig. 4D). The effect of changing the halogen from Cl to F is greater for YPO_4. This is especially true at high salinity, where the dissolved YPO_4 concentration is >1000 times higher in H_2O–NaF relative to H_2O–NaCl at $X_{salt} \geq 0.25$.

The solubility patterns are consistent with expectations derived from Pearson acid–base rules (Pearson 1997; Williams-Jones *et al.* 2012). Both Ce^{3+} and Y^{3+} are hard cations, but the greater hardness of Y^{3+} than that of Ce^{3+} should cause it to form more stable complexes with a hard ligand such as F^-. The greater solubility of YPO_4 than that of $CePO_4$ at fixed X_{NaF} bears this out. Similarly, Ce^{3+} and Y^{3+} should form more stable complexes with F^- than with Cl^- owing to the fluoride's hardness; again, this is the observed behavior (Fig. 4A,B). These observations are identical to those in dilute aqueous solutions at ambient conditions (Wood 1990), but differ from those at increased temperature along the H_2O liquid–vapor saturation curve (Migdisov *et al.* 2009), where the lower dielectric constant of H_2O is interpreted to lead to departures from Hard–Soft Acid–Base theory (Williams-Jones *et al.* 2012). In contrast, our results at high salt concentration and high P–T are in agreement with predictions from HSAB rules.

Solubility mechanism

The strong increase in the solubility of $CePO_4$ and YPO_4 with X_{NaF} at constant P and T implies the existence of a solution reaction involving only the NaF component from the fluid. The accelerating trend indicates that the ratio of solute mole fraction at a given NaF concentration to that in pure H_2O (X/X^o; Fig. 4C) rises steadily rather than maximizing and then declining. The simple dependence of

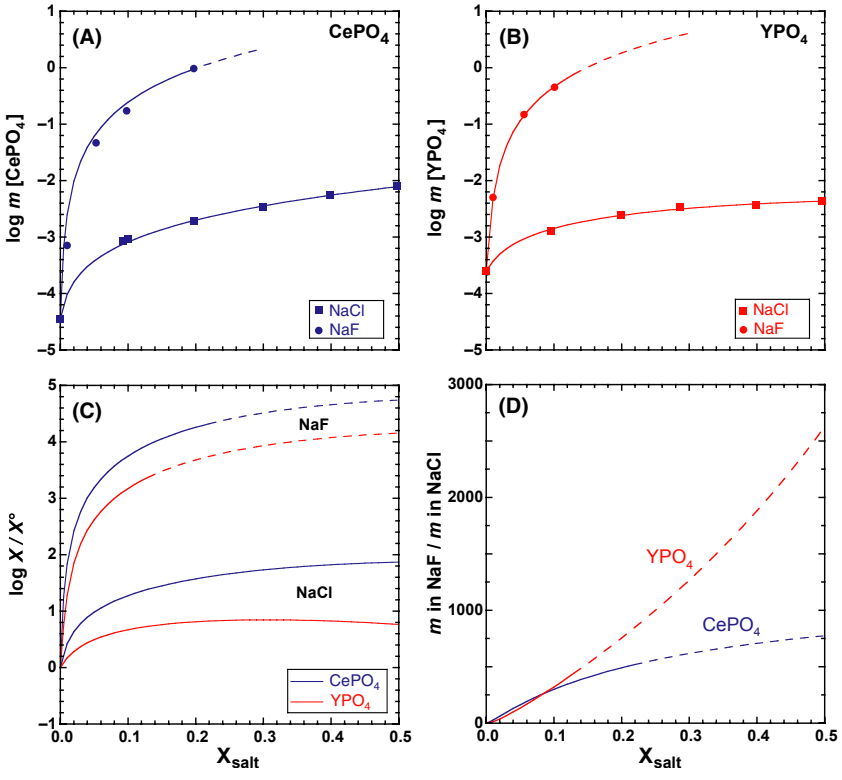

Fig. 4. Plot of (A) $CePO_4$ and (B) YPO_4 molality versus X_{NaCl} or X_{NaF} at 800°C and 1 GPa. The error bars (1σ) are also smaller than the symbol and are calculated based on the weighing uncertainties. (C) Plot comparing relative solubility enhancements (log X/X^0) on a mole-fraction basis as a function of salt mole fraction (X_{salt}). (D) Plot showing the relative effects of NaF versus NaCl solutions as a function of the ratio of the concentration m of $CePO_4$ and YPO_4 in NaF to the concentration m of $CePO_4$ and YPO_4 in NaCl for the same salt mole fraction (X_{salt}) in the solution. Data for NaCl solutions from Tropper *et al.* (2011).

both solubilities on X^2_{NaF} requires that H_2O is not involved in the dissolution reaction for either phosphate and that two solute products predominate in the solutions (Newton & Manning 2002, 2010). For $CePO_4$, the dissolution reaction must be very similar to that in H_2O–NaCl (Tropper *et al.* 2011), such as

$$CePO_4 + 2NaF = CeF_2^+ + Na_2PO_4^- \quad (1)$$

Following Eq. 1, the dissolution reaction for YPO_4 in H_2O–NaF must be:

$$YPO_4 + 2NaF = YF_2^+ + Na_2PO_4^- \quad (2)$$

Note, however, that this differs from the dissolution mechanism for the YPO_4 dissolution reaction in H_2O–NaCl solutions (Tropper *et al.* 2011):

$$YPO_4 + 2NaCl + H_2O = YCl(OH)_2 + NaH_2PO_4 \quad (3)$$

The stoichiometry and involvement of a mixed chloride–hydroxide species are required by the maximum attained at X_{NaCl} approximately 0.33 (Fig. 4C). Thus, the equivalent fluoride species, $YF(OH)_2$, must be less stable than $YCl(OH)_2$.

Ce–Y fractionation in NaCl–NaF brines

The experimental results indicate that salty solutions have the ability to fractionate Ce from Y at high P and T and that the nature of the fractionation depends strongly on the salt composition. Assuming that the $CePO_4$ solubility in H_2O at 800°C and 1 GPa is 0.04 millimolal (Table 1), the molar Ce/Y ratio in H_2O equilibrated with both minerals is 0.14. Figure 5 shows that as salt is added, the Ce/Y ratio in the fluid increases. However, in NaF solutions, the Ce/Y ratio reaches a constant value of 0.54 at low X_{NaF}. In contrast, the Ce/Y ratio increases steadily with rising X_{NaCl}. This is a consequence of the very different behavior of Y complexing in NaCl and NaF solutions. These results suggest that high P–T alkali halide brines can fractionate REE and significantly modify REE patterns by fluid–rock interaction.

Implications for REE transport F-bearing fluids in the deep crust

The results indicate that $CePO_4$ and YPO_4 solubilities may be very high in deep crustal fluids containing even small amounts of NaF. Taking Ce as representative of LREE, and Y of HREE, the results also indicate that the solubilities of HREE are much higher than those of LREE in NaF-bearing fluids. This contrasts with NaCl-bearing fluids, in which model LREE solubilities are greater than those of model HREE (Tropper *et al.* 2011). Although no direct measurements of F contents in granulite-facies fluid inclusions are available, the presence of F-bearing minerals

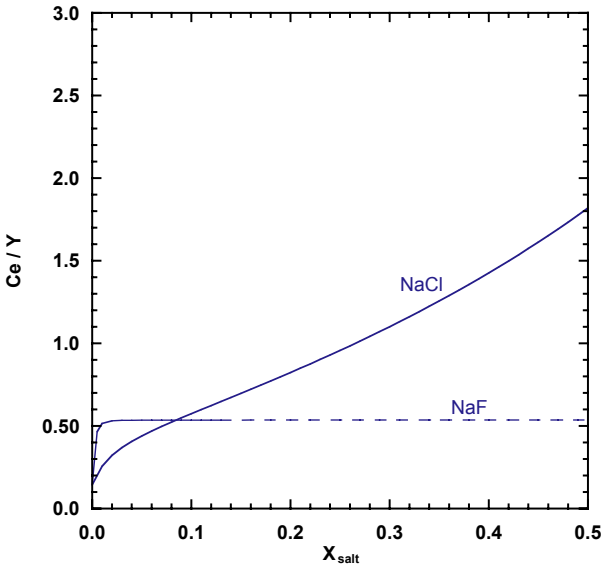

Fig. 5. Plot of Ce/Y ratio versus salt mole fraction (X_{salt}) showing the different behavior of Ce/Y in NaF and NaCl solutions.

(Pan & Fleet 1996; Pradeepkumar & Krishnanath 1996; Markl & Piazolo 1998; Tsunogae *et al.* 2003; Hansen & Harlov 2007), mass balance calculations (Pan & Fleet 1996), and solubility studies involving fluorite (Tropper & Manning 2007) together indicate that significant F contents may occur in high-grade metamorphic fluids. Further support for the interplay between F-rich fluids and rocks in deep crustal environments has been reported in charnockites from southern India, which contain fluorapatite as well as F-rich allanite, biotite, and hornblende (Hansen & Harlov 2007). Tsunogae *et al.* (2003) also attributed the formation of F-rich pargasites in the Napier Complex, East Antarctica, to be due to infiltration of F-bearing fluids during UHT metamorphism. Markl & Piazolo (1998) described the release of F-bearing fluids from syenites into the surrounding granulite-facies basement based on the F contents in biotite, tremolite, and humite, which allowed them to calculate fHF/fH_2O ratio. Pan & Fleet (1996) investigated the role of F during REE mobility and concluded that the presence of REE-bearing fluorapatite in granulites from the Superior Province, Ontario, Canada, was evidence that F-complexation might be a major mechanism for the transport of REE under granulite-facies conditions. These authors also observed an increase in the modal abundance of F-apatite in granulite-facies rocks, when compared to their amphibolite-facies precursors. In addition, whole-rock data and mass balance calculations also indicated an increase in REE and HFSE during prograde granulite-facies metamorphism.

Our experimental results reveal that the presence of a significant F component in granulite-facies fluids results in extremely high solubilities of Y + REE-bearing phosphate

compounds during lower crustal metamorphism. Significantly, the largest relative solubility increases occur at the lowest NaF concentration (Fig. 4C). Assuming F concentrations of approximately 1000 ppm F (Banks *et al.* 1994), our results indicate solubilities of approximately 0.06 and 0.30 millimolal Ce and Y, respectively. The data demonstrate that higher F concentrations will yield correspondingly greater enhancement. Most metamorphic brines will be dominated by a NaCl component, with F/Cl $\ll$ 1. The consequences for REE transport can be appreciated by considering that equilibration of NaCl brine (X_{NaCl} = 0.1) with fluorite at 800°C, 1 GPa, yields F concentrations of 0.336 m (Tropper & Manning 2007), or a molar F/(F + Cl) ratio of 0.052. Assuming this ratio in a NaF–NaCl–H_2O solution with X_{NaCl} = 0.1 at $CePO_4$ and YPO_4 saturation yields Ce and Y concentrations of 1.7 and 3.3 millimolal, respectively. These solubilities are greater than the 0.8 and 1.4 millimolal values that would hold for the F-free NaCl solution. Thus, even when the effects of low F/Cl are taken into account, the presence of F in high-grade NaCl-rich fluids significantly enhances REE solubility and mobility.

Although numerous field (Newton *et al.* 1998) and experimental (Hetherington *et al.* 2010; Harlov & Wirth 2012) studies have shown that REE mobility is greatly facilitated by the presence of brines, Harlov *et al.* (2006) have shown that fluid composition can affect LREE versus the (Y + HREE) mobility during localized, solid-state dehydration. In a 2-m-wide, charnockitic dehydration zone, Söndrum stone quarry, Halmstad, SW Sweden, Harlov *et al.* (2006) found that only (Y + HREE) were mobilized across the dehydration zone compared to the LREE. This suggested that the dominant halogen in the CO_2-rich fluids involved during the dehydration event was F as opposed to Cl. This is in agreement with our experimental results reported here and in Tropper *et al.* (2011), which demonstrate that the NaCl/NaF ratio in high *P*–*T* brines can dramatically impact the degree of LREE/HREE fractionation by the fluid phase (Fig. 5).

Implications for REE transport by subduction zone fluids

Plank *et al.* (2009) and Cooper *et al.* (2012) proposed that H_2O/Ce ratio in fluids liberated from subducting slabs is strongly temperature dependent and that this ratio is largely preserved through processes of transport and melting yielding an effective thermometer for slab–fluid reaction beneath volcanic arcs. However, this signal can be affected by increased concentrations of F or Cl in solution. Figure 6 shows that at 800°C, the H_2O/Ce ratio in fluids varies over many orders of magnitude due solely to the effect of salt concentration and identity. In each case, the effect of increasing salt concentration is to lower the H_2O/Ce ratio, which would give higher apparent temperatures of separation of fluid from a subducting slab. While concentrations of fluoride and chloride may generally be low, Fig. 6 shows that the greatest changes occur at the lowest salt concentrations. Notably, Cooper *et al.* (2012) found that H_2O/Ce ratio in melt inclusions from the Iraazu volcano was lower than would be expected for the predicted slab-top temperature in this system. They pointed to the increased F concentration in this magmatic system as a possible explanation. Our results lend support to this hypothesis.

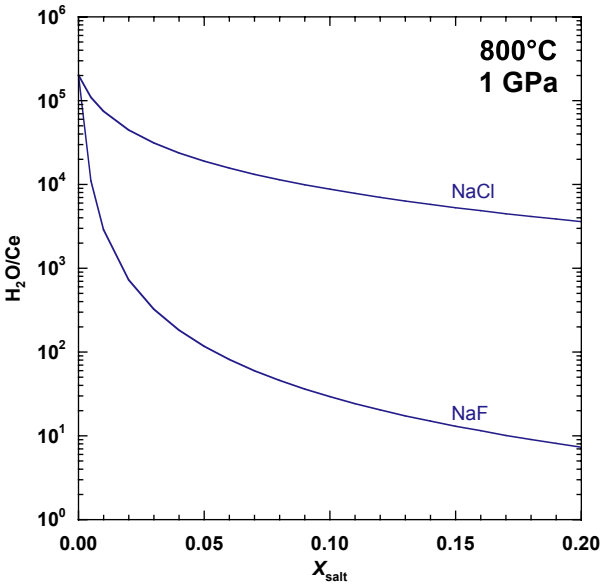

Fig. 6. Plot of the H_2O/Ce ratio in fluids versus the salt mole fraction (X_{salt}). The effect of increasing salt (NaCl, NaF) concentrations strongly lowers the H_2O/Ce ratio, thus resulting in higher apparent temperatures of fluid separation from a subducting slab.

CONCLUSIONS

(1) The solubilities of $CePO_4$ and YPO_4 are strongly enhanced by the addition of NaF to H_2O. With the addition of NaF, $CePO_4$ and YPO_4 solubilities rise to an increasing degree. Solubilities of $CePO_4$ and YPO_4 are greater than in pure H_2O by factors of 24 000 and 1800, respectively.

(2) The relative increases are substantially greater in NaF compared to NaCl. At a given salt concentration, both $CePO_4$ and YPO_4 are at least 10 times greater in NaF relative to NaCl, even at X_{salt} as low as approximately 0.02. The experimental results also indicate that salty solutions have the ability to fractionate Ce from Y at high *P* and *T* and that the nature of the fractionation depends strongly on the salt composition.

(3) Stoichiometric analysis of the solubility enhancements reveals that the dominant solute species of Ce and Y are anhydrous Ce- and Y-fluorides, consistent with the

simple dependence of both solubilities on X^2_{NaF}, which requires that H_2O is not involved.

(4) The results indicate that $CePO_4$ and YPO_4 solubilities are very high in deep crustal fluids containing even small amounts of NaF. Taking Ce as representative of LREE, and Y of HREE, the results also indicate that the solubilities of HREE are much higher than those of LREE in NaF-bearing fluids.

ACKNOWLEDGEMENTS

The authors wish to thank R. Newton for his generous help with the experiments. This study was supported by NSF grant EAR 1049901 to Manning. The helpful reviews of two anonymous journal referees and the editorial handling by Mark Person are also greatly appreciated.

REFERENCES

Agangi A, Kamenetsky VS, McPhie J (2010) The role of fluorine in the concentration and transport of lithophile trace elements in felsic magmas: insights from the Gawler Range Volcanics, South Australia. *Chemical Geology*, **273**, 314–25.

Andreoli MAG, Smith CB, Watkeys M, Moore JM, Ashwal LD, Hart RJ (1994) The geology of the Steenkampskraal monazite deposit, South Africa: implications for REE-Th-Cu mineralization in charnockite-granulite terranes. *Economic Geology*, **89**, 994–1016.

Antignano A, Manning CE (2008) Rutile solubility in H_2O, H_2O-SiO_2, and H_2O-$NaAlSi_3O_8$ fluids at 0.7-2.0 GPa and 700-1000 °C: implications for mobility of nominally insoluble elements. *Chemical Geology*, **255**, 283–93.

Ayers JC, Loflin M, Miller CF, Barton MD, Coath CD (2004) Dating fluid infiltration using monazite. In: *Proceedings of the Eleventh International Symposium on Water–Rock Interaction*, Vol. 1 (eds Wanty RB, Seal RR II), pp. 247–51. Balkeema Publishers, Lisse, the Netherlands.

Ayers JC, Watson EB (1991) Solubility of apatite, monazite, zircon and rutile in supercritical aqueous fluids with implications for subduction zone geochemistry. *Philosophical Transactions of the Royal Society A*, **335**, 365–75.

Banks DA, Yardley BWD, Campbell AR, Jarvis KE (1994) REE composition of an aqueous magmatic fluid: a fluid inclusion study from the Capitan Pluton, New Mexico, U.S.A. *Chemical Geology*, **113**, 259–72.

Bau M, Dulski P (1995) Comparative study of yttrium and rare-earth behaviors in fluorine-rich hydrothermal fluids. *Contributions to Mineralogy and Petrology*, **119**, 213–23.

Bohlen SR (1984) Equilibria for precise pressure calibration and a frictionless furnace assembly for the piston-cylinder apparatus. *Neues Jahrbuch für Mineralogie, Monatshefte*, **9**, 404–12.

Bohlen SR, Essene EJ (1978) The significance of metamorphic fluorite in the Adirondacks. *Geochimica and Cosmochimica Acta*, **42**, 1669–78.

Brennan J (1993) Partitioning of fluorine and chlorine between apatite and aqueous fluids at high pressure and temperature: implications for the F and Cl content of high-P-T fluids. *Earth and Planetary Science Letters*, **17**, 251–63.

Cetiner ZS, Wood SA, Gammons CH (2005) The aqueous geochemistry of the rare earth elements. Part XIV. The solubility of rare earth element phosphates from 23 to 150°C. *Chemical Geology*, **214**, 147–69.

Chakhmouradian AR, Wall F (2012) Rare earth elements: minerals, mines, magnets (and more). *Elements*, **8**, 333–40.

Constantopoulos J (1988) Fluid inclusions and rare earth element geochemistry of fluorite from south-central Idaho. *Economic Geology*, **83**, 626–36.

Cooper LB, Ruscitto DM, Plank T, Wallace PJ, Syracuse EM, Manning CE (2012) Global variations in H_2O/Ce: I. Slab surface temperatures beneath volcanic arcs. *Geochemistry, Geophysics, Geosystems*, **13**, Q03024.

Devidal JL, Gibert F, Kieffer B, Pin C, Montel JM (1998) A new method for solubility measurement: application to NdPO4 system in H2O-NaCl-HCl hydrothermal fluids. *Mineralogical Magazine*, **62**, 375–6.

Fayek M, Kyser TK (1997) Characterization of multiple fluid-flow events and rare-earth-element mobility associated with formation of unconformity-type uranium deposits in the Athabasca basin, Saskatchewan. *Canadian Mineralogist*, **35**, 627–58.

Haas JR, Shock EL, Sassani DC (1995) Rare earth elements in hydrothermal systems: estimates of standard partial molal thermodynamic properties of aqueous complexes of the rare earth elements at high pressures and temperatures. *Geochimica et Cosmochimica Acta*, **59**, 4329–50.

Hansen EC, Harlov DE (2007) Whole-rock, phosphate, and silicate compositional trends across an amphibolite- to granulite-facies transition, Tamil Nadu, India. *Journal of Petrology*, **48**, 1641–80.

Harlov DE, Wirth R (2012) Experimental incorporation of Th into xenotime at middle to lower crustal P–T utilizing alkali-bearing fluids. *American Mineralogist*, **97**, 641–52.

Harlov DE, Johansson L, Van Den Kerkhof A, Förster HJ (2006) The role of advective fluid flow and diffusion during localized, solid-state dehydration: Söndrum Stenhuggeriet, Halmstad, SW Sweden. *Journal of Petrology*, **47**, 3–33.

Harrison TM, Catlos EJ, Montel JM (2002) U–Th–Pb dating of phosphate minerals. *Reviews in Mineralogy and Geochemistry*, **48**, 523–58.

Hetherington CJ, Harlov DE, Budzyn B (2010) Experimental metasomatism of monazite and xenotime: mineral stability, REE mobility and fluid composition. *Mineralogy and Petrology*, **99**, 165–84.

Janots E, Engi M, Berger A, Allaz J, Schwarz O, Spandler C (2008) Prograde metamorphic sequence of REE minerals in pelitic rocks of the Central Alps: implications for allanite-monazite-xenotime phase relations from 250°C to 610°C. *Journal of Metamorphic Geology*, **26**, 509–26.

Jiang SY, Wang RC, Xu XS, Zhao KD (2005) Mobility of high field strength elements (HFSE) in magmatic-, metamorphic-, and submarine-hydrothermal systems. *Physics and Chemistry of the Earth*, **30**, 1020–9.

Klemme S (2004) Evidence for fluoride melts in Earth's mantle formed by liquid immiscibility. *Geology*, **32**, 441–4.

Lewis AJ, Palmer MR, Sturchio NC, Kemp AJ (1997) The rare earth element geochemistry of acid-sulphate and acid-sulphatechloride geothermal systems from Yellowstone National Park. *Geochimica et Cosmochimica Acta*, **61**, 695–706.

Manning CE, Boettcher SL (1994) Rapid-quench hydrothermal experiments at mantle pressures and temperatures. *American Mineralogist*, **79**, 1153–8.

Markl G, Piazolo S (1998) Halogen-bearing minerals in syenites and high-grade marbles of Dronning Maud Land, Antarctica: monitors of fluid compositional changes during late-magmatic

fluid–rock interaction processes. *Contributions to Mineralogy and Petrology*, **132**, 246–68.
Migdisov AA, Williams-Jones AE (2007) An experimental study of the solubility and speciation of neodymium (III) fluoride in F-bearing aqueous solutions. *Geochimica et Cosmochimica Acta*, **71**, 3056–69.
Migdisov AA, Williams-Jones AE, Wagner T (2009) An experimental study of the solubility and speciation of rare earth elements (III) fluoride- and chloride-bearing aqueous solutions at temperatures up to 300°C. *Geochimica et Cosmochimica Acta*, **73**, 7087–109.
Newton RC, Manning CE (2002) Experimental determination of calcite solubility in H_2O–NaCl solutions at deep crust/upper mantle pressures and temperatures: implications for metasomatic processes in shear zones. *American Mineralogist*, **87**, 1401–9.
Newton RC, Manning CE (2010) Role of saline fluids in deep-crustal and upper-mantle metasomatism: insights from experimental studies. *Geofluids*, **10**, 58–72.
Newton RC, Aranovich LY, Hansen EC, Vandenheuvel BA (1998) Hypersaline fluids in Precambrian deep-crustal metamorphism. *Precambrian Research*, **91**, 41–63.
Oreskes N, Einaudi MT (1990) Origin of rare earth element-enriched hematite breccias at the Olympic dam Cu–U–Au–Ag deposit, Roxby Downs, South Australia. *Economic Geology*, **85**, 1–28.
Pan Y, Fleet ME (1996) Rare element mobility during prograde granulite facies metamorphism: significance of fluorine. *Contributions to Mineralogy and Petrology*, **123**, 251–62.
Pearson RG (1997) *Chemical Hardness: Applications From Molecules to Solids*, 208 pp. Wiley-VCH, Weinheim.
Peterson JW, Chacko T, Kuehner SM (1991) The effects of fluorine on the vapour-absent melting of phlogopite + quartz: implications for deep-crustal processes. *American Mineralogist*, **76**, 470–6.
Plank T, Cooper L, Manning CE (2009) Emerging geothermometers for estimating slab surface temperatures. *Nature Geoscience*, **2**, 611–5.
Poitrasson F, Oelkers E, Schott J, Montel JM (2004) Experimental determination of synthetic NdPO4 monazite solubility in water from 21°C to 300°C: implications for rare earth element mobility in crustal fluids. *Geochimica et Cosmochimica Acta*, **68**, 2207–21.
Pollard PJ, Pichavant M, Charoy B (1987) Contrasting evolution of fluorine- and boron-rich tin systems. *Mineralium Deposita*, **22**, 315–21.
Pourtier E, Devidal JL, Gibert F (2010) Solubility measurements of synthetic neodymium monazite as a function of temperature ar 2 kbars, and aqueous neodymium speciation in equilibrium with monazite. *Geochimica et Cosmochimica Acta*, **74**, 1872–91.
Pradeepkumar AP, Krishnanath R (1996) Rare earth element mobility in halogenated aqueous fluids in the humite-marbles of Ambasamudram, Kerala Khondalite Belt, India. *Current Science*, **70**, 1066–74.
Rapp JF, Klemme S, Butler IB, Harley SL (2010) Extremely high solubility of rutile in chloride and fluoride-bearing metamorphic fluids: an experimental investigation. *Geology*, **38**, 323–6.
Rudnick RL, Barth M, Horn I, McDonough WF (2000) Rutile-bearing refractory eclogites: missing link between continents and depleted mantle. *Science*, **287**, 278–81.
Sallet R (2000) Fluorine as a tool in the petrogenesis of quartz-bearing magmatic associations: applications of an improved F–OH biotite-apatite thermometer grid. *Lithos*, **50**, 241–53.
Salvi S, Fontan F, Monchoux P (2000) Hydrothermal mobilization of high field strength elements in alkaline igneous systems: evidence from the Tamazeght Complex (Morocco). *Economic Geology*, **95**, 559–76.
Schmidt C, Rickers K, Bilderback DH, Huang R (2007) In situ synchrotron radiation XRF study of REE phosphate dissolution in aqueous fluids to 800°C. *Lithos*, **95**, 87–102.
Schwinn G, Markl G (2005) REE systematics in hydrothermal fluorite. *Chemical Geology*, **216**, 225–48.
Sengupta P, Raith MM, Datta A (2004) Stability of fluorite and titanite in a calc-silicate rock from the Vizianagaram area, Eastern Ghats Belt, India. *Journal of Metamorphic Geology*, **22**, 345–59.
Tropper P, Manning CE (2005) Very low solubility of rutile in H_2O at high pressure and temperature, and its implications for Ti mobility in subduction zones. *American Mineralogist*, **90**, 502–5.
Tropper P, Manning CE (2007) The solubility of fluorite in H_2O and H_2O–NaCl at high pressure and temperature. *Chemical Geology*, **242**, 299–306.
Tropper P, Manning CE, Harlov DE (2011) Solubility of $CePO_4$ monazite and YPO_4 xenotime in H_2O and H_2O–NaCl at 800 °C and 1 GPa: implications for REE and Y transport during high-grade metamorphism. *Chemical Geology*, **282**, 58–66.
Tsunogae T, Osanai Y, Owada M, Toyoshima T, Hokada T, Crowe WA (2003) High fluorine pargasites in ultrahigh temperature granulites from Tonagh Island in the Archean Napier Complex, East Antarctica. *Lithos*, **70**, 21–38.
Webster JD, Thomas R, Rhede D, Förster HJ, Seltmann R (1997) Melt inclusions in quartz from an evolved peraluminous pegmatite: geochemical evidence for strong tin enrichment in fluorine-rich and phosphorous-rich residual liquids. *Geochimica et Cosmochimica Acta*, **61**, 2589–604.
Williams ML, Jercinovic MJ, Hetherington CJ (2007) Microprobe monazite geochronology: understanding geologic processes by integrating composition and chronology. *Annual Review of Earth and Planetary Science*, **35**, 137–75.
Williams-Jones AE, Migdasov AA, Samson IM (2012) Hydrothermal mobilization of the rare earth elements – a tale of 'ceria' and 'yttria'. *Elements*, **8**, 355–60.
Wood SA (1990a) The aqueous geochemistry of the rare-earth elements and yttrium. 1. Review of available low-temperature data for inorganic complexes and the inorganic REE speciation of natural waters. *Chemical Geology*, **82**, 159–86.
Wood SA (1990b) The aqueous geochemistry of the rare-earth elements and yttrium. 1. Theoretical predictions of speciation in hydrothermal solutions to 350°C at saturation water vapor pressure. *Chemical Geology*, **88**, 99–125.
Yardley BWD (1985) Apatite composition and the fugacities of HF and HCl in metamorphic fluids. *Mineralogical Magazine*, **49**, 77–9.
Zhu C, Sverjensky DA (1992) F–Cl–OH partitioning between biotite and apatite. *Geochimica et Cosmochimica Acta*, **56**, 3435–67.